JDI Journal of Diabetes Investigation Open access
Official Journal of the Asian Association for the Study of Diabetes
ORIGINAL ARTICLE

Effect of adenosine monophosphate-activated protein kinase–p53–Krüppel-like factor 2a pathway in hyperglycemia-induced cardiac remodeling in adult zebrafish

Qiuyun Wang†, Chen Luo†, Guoping Lu, Zhenyue Chen*

Department of Cardiology, Ruijin Hospital, Shanghai Jiaotong University School of Medicine, Shanghai, China

Keywords
Adenosine monophosphate-activated protein kinases, Diabetic cardiomyopathies, Zebrafish

***Correspondence**
Zhenyue Chen
Tel.: +86-136-1190-2069
Fax: +86-21-6437-2614
E-mail address:
czy11203@rjh.com.cn

J Diabetes Investig 2021; 12: 320–333

doi: 10.1111/jdi.13393

ABSTRACT

Aims/Introduction: Diabetic cardiomyopathy is a type of myocardial disease. It causes left ventricular hypertrophy, followed by diastolic and systolic dysfunction, eventually leading to congestive heart failure. However, the underlying mechanism still requires further elucidation.

Materials and Methods: A high-glucose zebrafish model was constructed by administering streptozocin intraperitoneally to enhance the development of cardiomyopathy and then treated with adenosine monophosphate-activated protein kinase (AMPK) activator. Cardiac structure and function, and protein and gene expression were then analyzed. Cardiomyocytes (CMs) culture *in vitro* using lentivirus were used for detection of AMPK, p53 and Krüppel-like factor 2a (klf2a) gene expression.

Results: In the hyperglycemia group, electrocardiogram findings showed arrhythmia, echocardiography results showed heart enlargement and dysfunction, and many differences, such as increased apoptosis and myocardial fiber loss, were observed. The phospho-AMPK and klf2a expression were downregulated, and p53 expression was upregulated. Activation of phospho-AMPK reduced p53 and increased klf2a expression, alleviated apoptosis in CMs and improved cardiac function in the hyperglycemic zebrafish. *In vitro* knockdown system of AMPK, p53 and klf2a using lentivirus illustrated an increased p53 expression and decreased klf2a expression in CMs by inhibiting AMPK. Repression of p53 and upregulation of klf2a expression were observed, but no changes in the expression of AMPK and its phosphorylated type.

Conclusions: In the model of streptozocin-induced hyperglycemia zebrafish, the reduction of phosphorylated AMPK increased p53, which led to KLF2a decrease to facilitate apoptosis of CMs, inducing the cardiac remodeling and cardiac dysfunction. These results can be reversed by AMPK activator, which means the AMPK–p53–klf2a pathway might be a potential target for diabetic cardiomyopathy intervention.

INTRODUCTION

Heart failure in diabetes mellitus patients without any comorbidities, such as coronary artery disease and hypertension, was first defined by Rubler *et al.* in 1972, and this was referred to as diabetic cardiomyopathy (DCM), which is a general complication of diabetes mellitus[1,2]. DCM has become a serious public health issue in worldwide, and is associated with a high incidence of heart failure and mortality in diabetes patients. Mechanisms, such as inflammation, cardiomyocyte apoptosis, oxidative stress, myocardial fibrosis and mitochondrial dysfunction, have been reported to occur in the pathogenesis of DCM[3–5]. However, the underlying mechanism responsible for DCM still remains unclear and requires further elucidation.

Zebrafish are tropical fish that have recently emerged as a new and attractive model for studying physiological and

†These authors contributed equally to this work.

Received 27 March 2020; revised 7 August 2020; accepted 12 August 2020

pathological processes, and this is because of its high similarity to the human genome, transparent embryos and suitable for genetic manipulation[6,7]. The zebrafish animal model has been established as a disease model for cardiovascular diseases, and this is because of the fact that adult humans suffer from a high rate of cardiovascular diseases[8]. To date, there are several challenges posed in establishing the heart disease models in zebrafish, limiting their use in this field[9]. Streptozocin (STZ), a diabetogenic drug, induces diabetes mellitus and exerts a special function on cardiomyopathy in several animal models, and so zebrafish were used to establish a hyperglycemic model[10–13]. Sarras *et al.* reported that a type 1 diabetes mellitus model of adult zebrafish induced by STZ was applied in research that focused on tissue regeneration[13]. The underlying mechanisms of how STZ induces DCM in adult zebrafish still remain unclear.

Previous studies have documented that apoptosis of cardiomyocytes (CMs) has great significance in DCM[14,15]. Increased apoptosis of CMs in diabetic animal models or patients has been the leading cause of loss of contractile tissues, resulting in systolic and diastolic dysfunction[16,17]. Thus, inhibiting cardiomyocyte apoptosis can be an efficient way to inhibit myocardial remodeling in DCM[18–20].

Adenosine monophosphate-activated protein kinase (AMPK) plays a vital role in adenosine triphosphate-deprived conditions by sensing cell energy changes[21,22]. However, the role of AMPK in cell proliferation and apoptosis is more complex than originally thought, and often remains controversial. Guo *et al.*[23] showed that resveratrol relieves cardiac cell injury and apoptosis by activating AMPK. Recent studies have shown that AMPK regulates cell proliferation and apoptosis by phosphorylating and stabilizing the tumor suppressor, p53[24]. Krüppel-like factor 2a (klf2a), a member of the family of Cys2/His2 zinc-finger transcriptional factors, exerts an important function in cell proliferation and differentiation[25,26]. Wang *et al.*[27] showed that the levels of klf2a could affect deoxyribonucleic acid damage-induced apoptosis. AMPK, p53 and klf2a play vital roles in cardiovascular diseases, but the mechanism of progression in cardiomyopathy still requires extensive research.

Hence, in the present study, the hyperglycemia model was successfully established by STZ injection in zebrafish. The myocardial structural collapse and dysfunction of the heart in the hyperglycemic model showed that apoptosis plays an important role in the cardiac remodeling mechanism, participating in the pathogenesis of DCM. Furthermore, the activated AMPK pathway attenuates apoptosis in CMs, and restores structural collapse and dysfunction of the heart in the model. The *in vitro* knockdown system of AMPK, p53 and klf2a using lentivirus has shown an upstream and downstream relationship among them. Above all, these results suggested that inhibition of myocardial cell apoptosis by activating the AMPK–p53–klf2a pathway might be a potential method for treating DCM.

METHODS

Zebrafish care and husbandry

The adult AB strain zebrafish (*Danio rerio*) were maintained in the laboratory of Rui Jin Hospital, Shanghai Jiao Tong University School of Medicine. The fish were maintained in water for 10 h dark and 14 h light cycle at a temperature of 28.5°C. The fish used in the present study were approximately 15–18 months-of-age and were randomly chosen from different clusters. The experiments were carried out according to the approved ethical principles provided by the Rui Jin Hospital Animal Care and Use Committee animal protocols.

STZ injection

STZ (S0130; Sigma, St. Louis, MO, USA) was administered through intraperitoneal injection by using a 29-G insulin syringe needle. After that, 0.3% STZ was dissolved in 0.09% NaCl and 350 mg/kg (70–150 μL dependent on weight) on days 1, 3 and 5. The control fish were injected with the same volume of 0.09% NaCl solution on days 1, 3 and 5. The corresponding indexes were detected on days 7, 14 and 21.

A-769662 injection

Zebrafish (aged 15–18 months) were randomly selected, followed by administration of 0.16 mg/mL tricaine liquid anesthesia to cease the whole-body activity, and the anesthesia time was approximately 3 min and 40 s, A–769662 (Gene Operation, ISY1061). Next, phosphate-buffered saline 1:1 dilution with 50% dimethyl sulfoxide was injected by using a 28.5-G insulin syringe needle intraperitoneally at a dose of 100 μg/g on days 2, 4 and 6. The zebrafish in the normal control group were injected with a similar volume of 0.09% NaCl on days 2, 4 and 6. Zebrafish were also tested on days 7, 14 and 21.

Glucose measurements

The zebrafish were anesthetized with 0.16 g/L of tricaine (MS-222; SIGMA-ALDRICH, St. Louis, MO, USA), the blood (1–2 μL) from each fish was harvested, and then, the blood glucose was measured using the glucose (HK) assay kit (DIGL-200; BioAssay Systems, Taichung City, Taiwan, China) according to the manufacturer's instructions.

Western blot analysis

Primary antibodies, such as anti-cleaved P53 (ab1101; Abcam, Shanghai, China), anti-AMPK alpha 1 (ab32047; Abcam), anti-KLF2 (ab203591; Abcam) and anti-glucose transporter (GLUT) 12 (ab75441; Abcam) were obtained. The anti-glyceraldehyde 3-phosphate dehydrogenase (GAPDH; DH0261#) was purchased from Donghuan Biotech Co., Ltd (Shanghai, China). All antibodies were diluted according to the manufacturer's instructions, and immunoreactivity was visualized using a chemiluminescence detection kit (DH0101). Dissection of zebrafish cardiac muscle was manually homogenized and then lysed in tissue lysis buffer with protease inhibitor (Roche, Basel, Switzerland).

Ribonucleic acid extraction and quantitative real-time polymerase chain reaction

Total ribonucleic acid (RNA) from cultured cells or tissues was extracted using Trizol reagent according to the manufacturer's instructions. The total RNA was measured by a NanoDrop ND-1000 spectrophotometer (Thermo Scientific, Waltham, MA, USA) and retrotranscribed immediately by the FastQuant RT Super Mix (KR108; TIANGEN Biotech, Beijing, China). Quantitative polymerase chain reaction (qPCR) was used with ABI PRISM 7500 fast real-time PCR system (Applied Biosystems, Foster City, CA, USA) and the SuperReal PreMix (FP204; TIANGEN Biotech). GAPDH messenger RNA was considered the control. The primers for AMPK in quantitative real-time PCR experiments were as follows: the forward primer F; 5′-GGATC TTCTTCACGCCTCAG-3′, and reverse primer R; 5′- TCCTC CCGAATCTCTTTG ATG-3′. Primers for p53 were the forward primer F; 5′-ATAAGAGTG GAGGGCAATCAGCGA-3′, and reverse primer R; 5′-AGTGATGATTGTGAGGATGGGCCT-3′. Primers for Klf2 were the forward primer F; 5′-CAGAATAACA-GACGACGAAGA-3′, and reverse primer R; 5′-CGAGTCCGA-GATTGTCAGA-3′. Primers for GLUT12 were the forward primer F; 5′-TACGGACGACGCTTACCAT-3′, and reverse primer R; 5′-GCCACTGACATCCCAACCA-3′.

Immunostaining and fluorescence microscopy

The hearts were fixed in 4% paraformaldehyde, embedded in paraffin, sectioned into 5-μm thick slices and then underwent immunofluorescence[28]. Antibodies used in this experiment included anti-MEF2 (sc-17785; Santa Cruz Biotechnology; Santa Cruz, CA, USA) and anti-proliferating cell nuclear antigen (ab32047; Abcam). All antibodies were diluted according to the manufacturer's instructions. The images obtained were visualized under an OLYMPUS DP70 microscope (Tokyo, Japan).

Terminal deoxynucleotidyl-transferase-mediated dUTP nick-end-labeling assay

The hearts were fixed with 4% paraformaldehyde, embedded in paraffin and cut into 5-μm thick slices. The CMs that underwent different treatments were placed on a glass. Terminal deoxynucleotidyl-transferase-mediated dUTP nick-end-labeling (TUNEL) assays were operated using the *In Situ* Cell Death Detection Kit (Roche) according to the manufacturer's protocol.

Transmission electron microscopy

The heart tissues were fixed in 2.5% glutaric dialdehyde for approximately 4 h and washed three times with 0.1 mL phosphate buffer. Next, the samples were embedded in Epon 812 and cut into 100-nm thick slices using UC7 Ultramicrotome (Leica, Heerbrugg, Switzerland). The sections were then stained with uranyl acetate and lead citrate, and the images were captured by using an electron microscopy core facility with Philips (Amsterdam, the Netherlands) CM-120 TEM (Amsterdam, the Netherlands).

Electrocardiogram and echocardiography

Electrocardiogram (ECG) and echocardiography were operated as described previously[29], and the fish were anesthetized as described previously[30]. The fish were fixed and placed by facing the ventral side upwards and gently squeezing the caudal fin. ECG was recorded after stabilizing for 2 min using the BIOPAC ECG100C System (Goleta, CA, USA). ECG was measured and statistically analyzed, which was as follows: the amplitude of QRS-wave alternating between high and low was referred to as "voltage alteration"; the ST-T depression or T-wave inversion was defined as "ST-T change"; and the "prolonged P-P interval" was referred to as the "sinus arrest". For echocardiography, imaging was carried out in the short axis (i.e., perpendicular to the fish) and long axis (i.e., parallel to the fish) using an MS-550S transducer (VisualSonics, Toronto, Canada) coupled to a 50-MHz ultrasound probe. The ejection fraction (EF) was calculated by the formula, (end-diastolic volume minus end-systolic volume) / end-diastolic volume. The time parameters, including isovolumic relaxation time (IVRT), ventricular ejection time (VET) and isovolumetric contraction time (IVCT) were calculated, and the parameters after adjusting the heart rate (HR; IVRTa, VETa and IVCTa, respectively) represent the percentage of heartbeat time.

Primary CM culture

The CMs from the ventricles were obtained for the study[31]. CMs were cultured in L-15 media supplemented with 10% fetal bovine serum and 1% penicillin/streptomycin. The CMs were maintained in a humidified atmosphere at 28.5°C containing 5% CO_2.

Plasmid construction production of lentivirus and cell infection

The specific short hairpin RNAs (shRNA) against P53, klf2a, prkaa1 and control shRNA were designed and synthesized by GenePharma (Shanghai, China). The shRNAs were ligated into the AgeI/EcoRI sites in the lentiviral vector pLKO.1. DanioShP53: sense: CCGGGCAATCAGCG AGCAAATTACA CTCGAGTGTAATTTGCTCGCTGATTGCTTTTTG; Daniosh KIF2: sense: CCGGGCCACTATCTCTCCAGGAATGCTCGA GCATTCCTGGAGAGATAGTGGCTTTTTG;Danioshprkaa1: sense: CCGGGCAGGATCTTCCCAAGTATCTCTCGAGAGA TACTTGGGAA GATCCTGCTTTTTG.

The shuttle vectors and HEK 293T cells were transiently transfected using Lipofectamine 2000 (Invitrogen, Waltham, MA, USA) according to the protocol. Medium containing the virus was harvested and filtered after 72 h of transfection, and was used for further research.

Statistical analysis

All data are expressed as the mean ± standard deviation, and each experiment was repeated at least three times. $P < 0.05$ was considered to be significant, whereas $P < 0.01$

represented a highly significant difference in a two-tailed Student's *t*-test.

RESULTS

STZ induces hyperglycemia model in zebrafish

Previous studies have shown that STZ treatment induced DCM in several animal models. To determine whether STZ induces hyperglycemia in zebrafish, STZ 350 mg/kg was administered intraperitoneally[32]. The blood glucose levels of zebrafish in the STZ-injected group were significantly increased the next day, and high levels were maintained until 30 days without intervention (Figure 1a). The zebrafish had a fasting plasma glucose level of ≥200 mg/dL, which was considered hyperglycemic[33]. Previous studies reported that the GLUT family, which are the main carriers of glucose, was involved in cell apoptosis through regulating p53[34,35]. Our qPCR and western blot analysis results showed a significant decrease in the expression of GLUTs, such as GLUT1, GLUT2 and GLUT12, in the hyperglycemic fish group (Figure 1b,c). In addition, the number of zebrafish was counted daily, and zebrafish in both groups before treatment showed a 100% survival rate. The fish count was recorded after every 3 days in each group, and the survival of zebrafish in the hyperglycemia group was decreased when compared with the control group ($P < 0.01$; Figure 1d). Furthermore, the weight

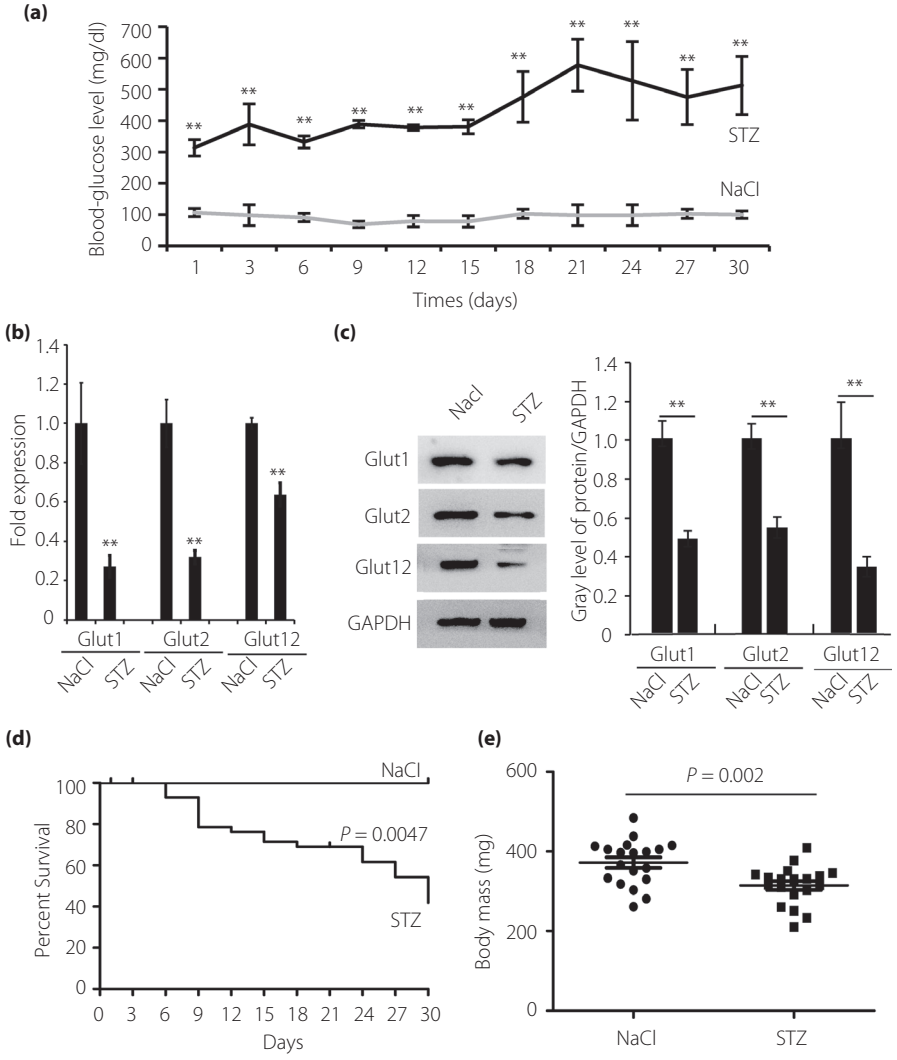

Figure 1 | Streptozocin (STZ) induces hyperglycemia in zebrafish. (a) Blood glucose assay analysis of blood glucose *in vivo* continues for 30 days. The fish were injected with STZ in a dose of 350 mg/kg and maintained in different days. Values >200 mg/dL were considered hyperglycemic. (b) Quantitative polymerase chain reaction analysis of glucose transporter (GLUT)1, GLUT2 and GLUT12 in hyperglycemic zebrafish hearts. Glyceraldehyde 3-phosphate dehydrogenase (GAPDH) was measured as the control. (c) Western blot analysis of GLUT1, GLUT2 and GLUT12 in hyperglycemic zebrafish injected with STZ. GAPDH was used as the control. (d) Survival analysis of the hyperglycemic fish and control fish in 30 days. (e) Body mass analysis of the hyperglycemia zebrafish model. Each experiment was repeated a minimum of three times. **Highly significant difference ($P < 0.01$) in a two-tailed Student's *t*-test.

of zebrafish in both groups was measured on day 21, and the fish injected with STZ lost weight compared with the control group (Figure 1e).

Expression of AMPK, p53 and klf2a in the heart of hyperglycemic zebrafish

A previous study showed that AMPK regulation could affect apoptosis in CMs and a hyperglycemic zebrafish model[36]. Thus, to elucidate the possible mechanism of DCM, the expression levels of components of the AMPK pathway were examined in our models. Western blotting results showed that the protein levels of phospho-AMPK and klf2a were reduced, but the expression of p53 was elevated in the STZ-induced DCM (Figure 2b). Recently, many compounds have been found to activate AMPK, such as A769662, 5-amino-imidazol-4-carboxamide-1-b-4-ribofuranoside, non-steroidal anti-inflammatory drugs and so on[37]. In the present study, A769662 was used and increased the phosphorylation level of AMPK and the expression of klf2a, whereas p53 was suppressed (Figure 2a,b).

Hyperglycemia induces muscular disarray, myofibril loss, vacuolization, mitochondrial condensation and apoptosis activation

In the present study, transmission electron microscopy analysis confirmed muscular disarray and myofibril loss in the hearts of hyperglycemic zebrafish. Meanwhile, vacuolization and mitochondrial condensation were found in the hearts (Figure 3a). Previous work documented apoptosis as one of the main causes of DCM, and so hematoxylin–eosin, TUNEL and western blotting were carried out to assess the apoptosis in the zebrafish model of DCM. Hematoxylin–eosin staining showed marked muscular disarray, myofibril loss and reduced myocardial density in the heart of hyperglycemic fish (Figure 3b). TUNEL assay showed that the apoptosis was increased in the hearts of hyperglycemic fish hearts when compared with the control group (Figure 3c).

Hyperglycemia induces cardiac dysfunction in adult zebrafish

ECG was carried out to detect the hyperglycemia-induced electrophysiological changes in the myocardium of zebrafish, and

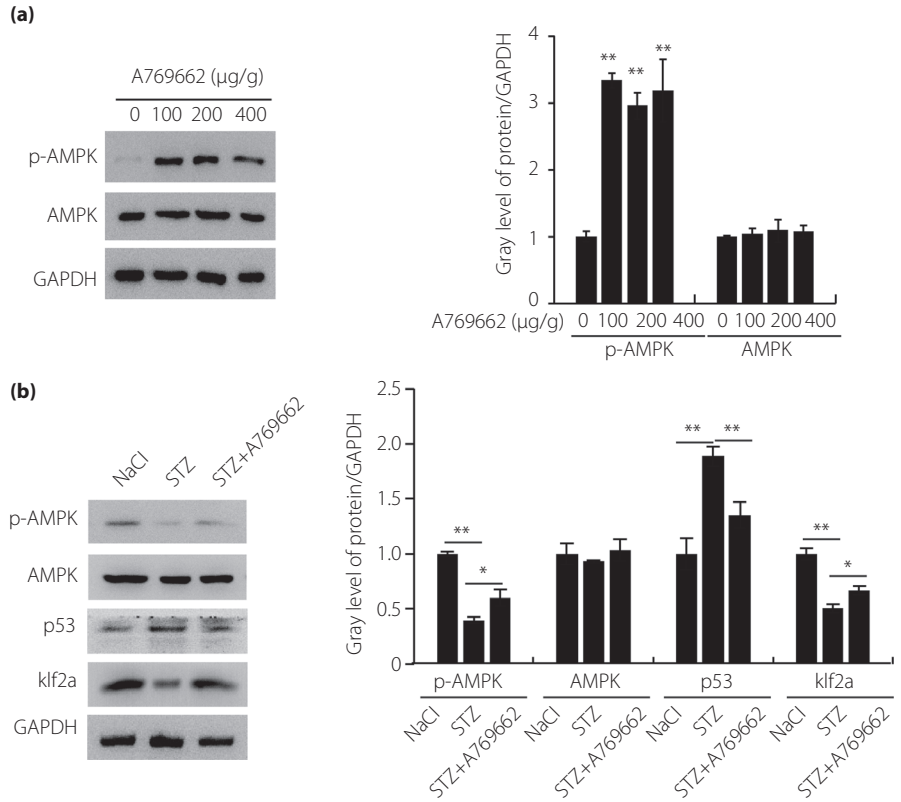

Figure 2 | The adenosine monophosphate-activated protein kinase (AMPK) pathway was involved in the hyperglycemic zebrafish. (a) Real-time polymerase chain reaction and western blot analysis of the expression of AMPK in different concentrations of A769662 (n = 21 fish per group). (b) Real-time polymerase chain reaction and western blot analysis of the expression of AMPK, p53 and Krüppel-like factor 2a (klf2a) in hyperglycemic zebrafish and A769662 intervention zebrafish compared with the control group (n = 21 fish per group). Each experiment was repeated a minimum of three times. *Statistically significant difference ($P < 0.05$), **Highly significant difference ($P < 0.01$) in a two-tailed Student's t-test. GAPDH, glyceraldehyde 3-phosphate dehydrogenase; p-AMPK, phospho-adenosine monophosphate-activated protein kinase; STX, streptozocin.

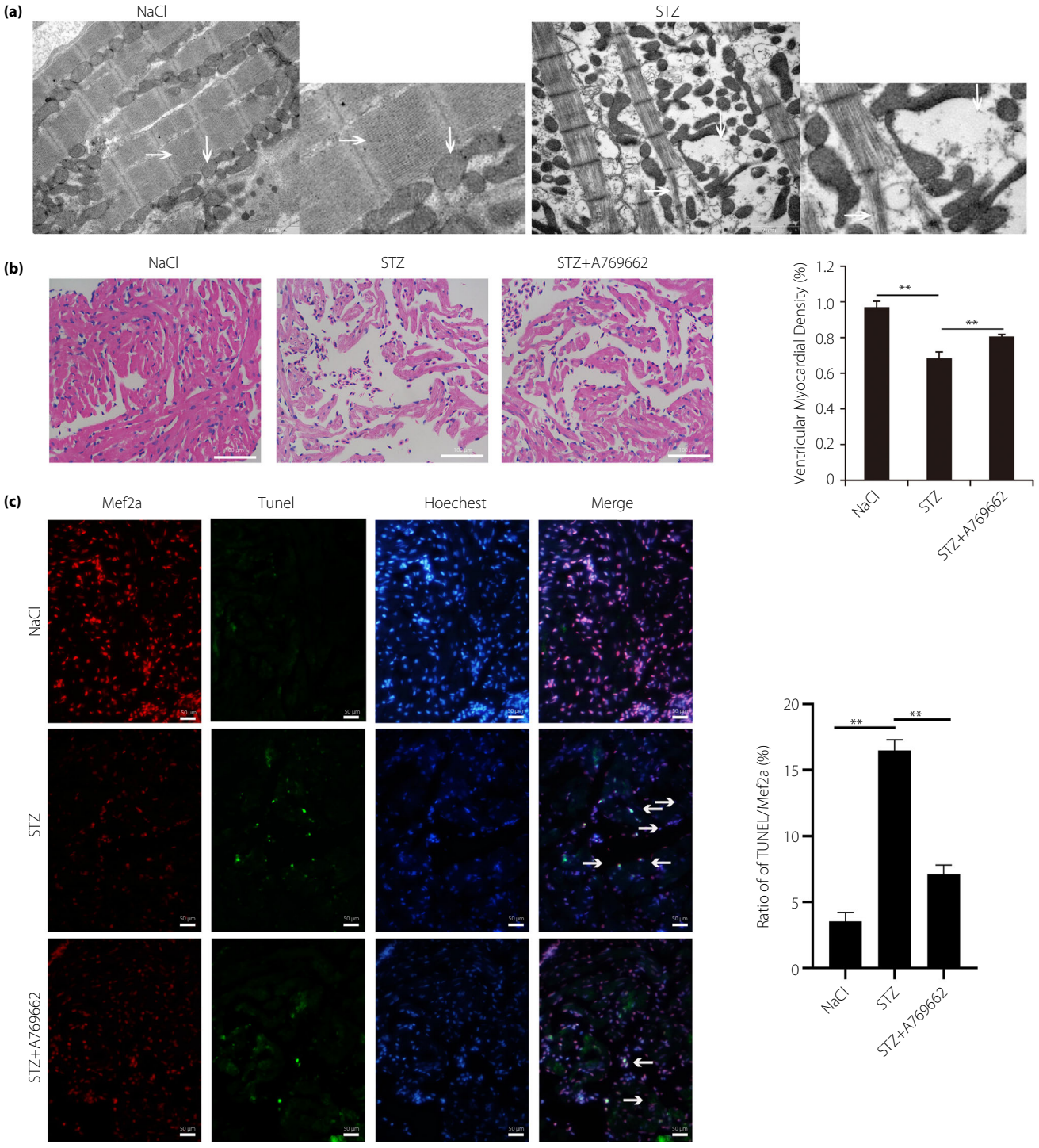

Figure 3 | Hyperglycemia induced muscular disarray, myofibril loss, vacuolization, mitochondrial condensation and apoptosis activation. (a) Transmission electron microscopy image verified muscular disarray, myofibril loss, vacuolization and mitochondrial condensation in hyperglycemic zebrafish compared with the control group (n = 21 field, repeated five times); scale bars, 2 μm. (b) Hematoxylin–eosin staining analysis of the heart in hyperglycemic zebrafish and A769662 intervention zebrafish compared with the control group after 21 days; scale bars, 100 μm. Quantification analysis of ventricular myocardial density in hematoxylin–eosin-stained hearts between the three groups. (c) Terminal deoxynucleotidyl-transferase-mediated dUTP nick-end-labeling (TUNEL) assay analysis of cell apoptosis in the heart of hyperglycemia zebrafish and A769662 intervention zebrafish compared with the control group zebrafish; scale bars, 50 μm. Each experiment was repeated a minimum of three times. **Highly significant difference ($P < 0.01$) in a two-tailed Student's t-test. STX, streptozocin.

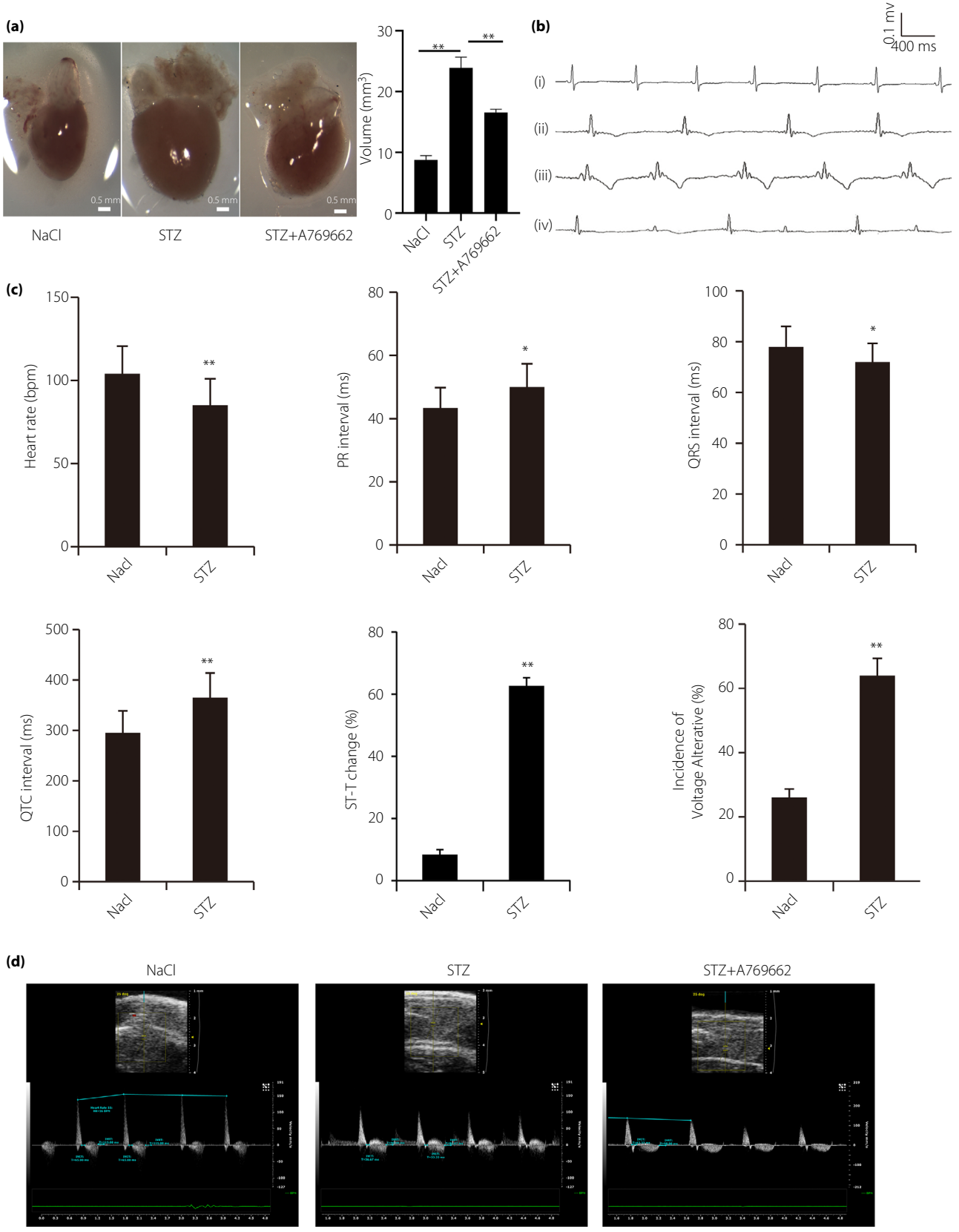

Figure 4 | Cardiac dysfunction was involved in hyperglycemic zebrafish. (a) Streptozocin (STZ) treatment induces enlarged heart in zebrafish, which is partially canceled by A769662, adenosine monophosphate-activated protein kinase activator; scale bar, 0.5 mm. (b) Typical electrocardiogram diagram; (i) normal electrocardiogram; (ii) escape rhythm representative diagram; (iii) T-wave inversion; and (iv) "voltage alternation" diagram. (c) Electrocardiogram parameters were significantly different in the two groups, such as heart rate, PR interval, QRS interval, QTc interval, ST-T change and voltage-alterative. (d) Typical B-mode echocardiography images of hyperglycemic zebrafish, control zebrafish and A769662 intervention zebrafish to evaluate ventricular morphology and function. Image data were automatically generated using the Vevo 2100 Workstation Software package (VisualSonics, Toronto, Canada). (n = 21 fish). *P < 0.05, **P < 0.01 compared with the wild-type group.

the results showed a marked decrease in the HR of hyperglycemia fish. The incidence of "ST-T change" and "voltage alternation" in hyperglycemia fish was markedly increased. However, the PR and QT intervals after adjusting the HR showed no significant differences (Figure 4c). A normal ECG recording from the untreated fish is shown in Figure 4b(i). The representative diagram of escape rhythm is shown in Figure 4b(ii), representative T-wave inversion is shown in Figure 4b(iii). Other abnormal ECG changes, such as "voltage alternation", is shown in Figure 4b(iv).

Echocardiographic parameters showed significant differences between the hyperglycemia group and control group (Table 1). The B-mode echocardiography images are presented in 4-D. The ventricular function and morphology were automatically generated using the Vevo 2100 Workstation Software package (Toronto, Canada).

Cardiac function was dynamically monitored by echocardiography, and the results showed that the stroke volume (SV), cardiac output (CO) and EF in the hyperglycemia group were lower than those in the control group. After 14 days of STZ intervention, the IVRT adjusted by HR (IVRTa) of the zebrafish in the hyperglycemia group was shorter than the control group, which indicated that the diastolic function was impaired, while the systolic function showed no significant change. After 21 days of STZ intervention, a significant reduction of SV and EF showed impaired myocardial contractility and systolic dysfunction (Tables 1 and 2). Systolic indices showed shortened VET adjusted by HR (VETa) and IVCT adjusted by HR (IVCTa) in hyperglycemia group. Furthermore, a significant reduction of HR and SV contributed to decreased CO. The remarkable decrease in EF was used to estimate the cardiac function, showing an impaired systolic function in the hyperglycemic zebrafish (Table 1).

In addition, echocardiography was carried out to examine the effect of A769662 on the hearts of hyperglycemic zebrafish. After treatment with A769662, the echocardiography results

Table 1 | Doppler echocardiography measurement in the hyperglycemic zebrafish

	Wild-type (n = 21)	STZ-treated 7 days (n = 21)	STZ-treated 14 days (n = 21)	STZ-treated 21 days (n = 21)
IVCT (ms)	40.57 ± 6.831	38.276 ± 6.787	37.373 ± 6.845	31.010 ± 5.769**
IVCTa (%)	5.5 ± 1.4	5.1 ± 0.9	5.1 ± 1.3	4.2 ± 0.9**
VET (ms)	232.548 ± 36.197	229.752 ± 30.654	224.710 ± 36.845	220.643 ± 37.459
VETa (%)	32.0 ± 8.1	30.9 ± 5.7	30.4 ± 6.8	30.0 ± 7.4
E (mm/s)	25.737 ± 11.547	34.477 ± 9.112**	35.619 ± 8.235**	38.431 ± 8.687**
A (mm/s)	123.994 ± 39.484	121.369 ± 20.476	117.764 ± 26.910	116.459 ± 26.403
E/A	0.205 ± 0.039	0.285 ± 0.067**	0.304 ± 0.032**	0.332 ± 0.049**
IVRT (ms)	91.133 ± 16.042	90.805 ± 16.117	85.443 ± 9.199*	82.238 ± 8.401*
IVRTa (%)	12.4 ± 2.9	12.1 ± 1.8	11.6 ± 2.1	11.1 ± 1.6
SV (μL)	0.270 ± 0.095	0.263 ± 0.061	0.259 ± 0.046	0.255 ± 0.054
EF (%)	50.379 ± 5.106	47.268 ± 8.081	45.648 ± 7.093*	40.063 ± 8.154**
CO (μL/min)	21.709 ± 7.434	21.586 ± 7.053	21.143 ± 5.290	20.858 ± 5.958
Volume s (μL)	0.264 ± 0.054	0.326 ± 0.049**	0.343 ± 0.058**	0.369 ± 0.06**
Volume d (μL)	0.533 ± 0.114	0.627 ± 0.124*	0.666 ± 0.068**	0.674 ± 0.094**

Values are the mean ± standard deviation, n = 21 in each group. *P < 0.05 and **P < 0.01 as compared with wild-type zebrafish. Image data were automatically generated using the Vevo 2100 Workstation Software package. A, A-wave peak velocity; E, E-wave peak velocity; E/A, E to A ratio; EF, ejection fraction defined as (end-diastolic volume minus end-systolic volume) / end-diastolic volume; IVCT, isovolumic contraction time; IVCTa, adjusted isovolumic contraction time, calculated by the formula, isovolumic contraction time ms / (60 s × 1000 / heart rate) × 100%; IVRT, isovolumic relaxation time; IVRTa, adjusted isovolumic relaxation time, calculated by the formula, isovolumic relaxation time ms / (60 s × 1000 / heart rate) × 100%; STZ, streptozocin; VET, ventricular ejection time; VETa, adjusted ventricular ejection time, calculated by the formula, ventricular ejection time ms / (60 s × 1000/HR) × 100%; Volume d, end-diastolic volume; Volume s, end-systolic volume.

Table 2 | Doppler echocardiography results after treatment with A769662 in the hyperglycemic zebrafish

	n (*n* = 21)	STZ (*n* = 21)	STZ + A769662 (*n* = 21)
IVCT (ms)	41.762 ± 6.518	31.024 ± 6.904**	38.300 ± 12.353*
IVCTa (%)	5.8 ± 1.1	4.2 ± 1.3**	5.2 ± 1.4*
VET (ms)	230.692 ± 54.900	220.875 ± 41.426	237.678 ± 41.536
VETa (%)	32.2 ± 9.8	29.6 ± 6.8	32.4 ± 4.2
E (mm/s)	25.643 ± 7.607	38.648 ± 13.277**	31.531 ± 12.130
A (mm/s)	125.714 ± 21.648	116.786 ± 40.499	133.297 ± 25.144
E/A	0.203 ± 0.047	0.337 ± 0.073**	0.249 ± 0.126**
IVRT (ms)	91.905 ± 23.076	82.286 ± 11.032*	90.238 ± 16.791
IVRTa (%)	12.7 ± 3.2	11.1 ± 2.5	12.3 ± 1.8
SV (μL)	0.271 ± 0.100	0.256 ± 0.079	0.266 ± 0.085
EF (%)	51.0 ± 6.2	40.6 ± 9.1 **	48.1 ± 10.9*
CO (μL/min)	22.672 ± 8.777	20.111 ± 5.225	21.404 ± 5.183
Volume s (μL)	0.262 ± 0.049	0.376 ± 0.055 **	0.305 ± 0.091**
Volume d (μL)	0.533 ± 0.132	0.681 ± 0.115**	0.614 ± 0.208

Values are the mean ± standard deviation, $n = 21$ in each group. *$P < 0.05$ and **$P < 0.01$ as compared with wild-type zebrafish. Image data were automatically generated using the Vevo 2100 Workstation Software package. A, A-wave peak velocity; E, E-wave peak velocity; E/A, E to A ratio; EF, ejection fraction defined as (end-diastolic volume minus end-systolic volume)/end-diastolic volume; IVCT, isovolumic contraction time; IVCTa, adjusted isovolumic contraction time, calculated by the formula, isovolumic contraction time ms/(60 s × 1000/HR) × 100%. IVRT, isovolumic relaxation time; IVRTa, adjusted isovolumic relaxation time, calculated by the formula, isovolumic relaxation time ms / (60 s × 1000/HR) × 100%; STZ, streptozocin; VET, ventricular ejection time; VETa, adjusted ventricular ejection time, calculated by the formula, ventricular ejection time ms / (60 s × 1000/HR) × 100%; Volume d, end-diastolic volume; Volume s, end-systolic volume.

showed that the SV, CO and EF were improved in the hyperglycemic fish group, IVRTa also showed significant prolongation than the untreated hyperglycemia group, and the diastolic function was improved as well (Table 2). The volume and the end-diastolic volume were restored in hyperglycemia fish model after activating AMPK consistently along with the enlargement of the heart (Figure 4a; Table 1). While TUNEL assay showed that A769662 alleviated the STZ-induced apoptosis in the hyperglycemic fish heart (Figure 3c), which was consistent with the echocardiography results above. These findings suggested that STZ could induce DCM in zebrafish, and activation of AMPK by A769662 could inhibit cardiac remodeling.

AMPK–p53–klf2a pathway is involved in hyperglycemia zebrafish cardiomyocytes

To further confirm the inhibition of AMPK–p53–klf2a pathway by hyperglycemia, the expression of the AMPK pathway was detected in hyperglycemic zebrafish CMs cultured *in vitro*. As expected, activation of AMPK *in vitro* inhibited the expression of p53 and increased klf2a (Figure 5a,b). Furthermore, qPCR analysis showed that A769662 restored STZ-induced repression of GLUT1, GLUT2 and GLUT12 (Figure 5c). In addition, AMPK activation alleviated STZ-induced apoptosis in CMs (Figure 5d), which was consistent with the results obtained *in vivo*.

The above data showed that the AMPK–P53–klf2a pathway was involved in the hyperglycemic zebrafish CMs model. Thus, it was necessary to identify the relationships among them. The primary cultured CMs of zebrafish were isolated and cultured, followed by suppressing the expressions of AMPK, p53 and klf2a by shRNA that are specific to them, respectively. qPCR and western blotting results showed that AMPK and klf2a expression were inhibited, and p53 expression was elevated in cells transfected with shAMPK (Figure 6a,b). Furthermore,

Figure 5 | Adenosine monophosphate-activated protein kinase (AMPK)–p53–Krüppel-like factor 2a (klf2a) pathway involved in hyperglycemic zebrafish cardiomyocytes. (a) Real-time polymerase chain reaction and western blot analysis of the expression of AMPK in hyperglycemic and control zebrafish cardiomyocytes, and control with A769662 intervention *in vitro*. (b) Real-time polymerase chain reaction analysis of the expression of p53 and klf2a in hyperglycemic and control zebrafish cardiomyocytes, and control with A769662 intervention *in vitro*. (c) Real-time polymerase chain reaction analysis of the expression of glucose transporters (Glut) in hyperglycemic and control zebrafish cardiomyocytes, and control with A769662 intervention *in vitro*. (d) Terminal deoxynucleotidyl-transferase-mediated dUTP nick-end-labeling (TUNEL) assay analysis of cell apoptosis in hyperglycemic and control zebrafish cardiomyocytes, and control with A769662 intervention cardiomyocytes cultured *in vitro*; scale bars, 100 μm. Each experiment was repeated a minimum of three times. *Statistically significant difference ($P < 0.05$), **Highly significant difference ($P < 0.01$) in a two-tailed Student's *t*-test. p-AMPK, phospho-adenosine monophosphate-activated protein kinase; STX, streptozocin.

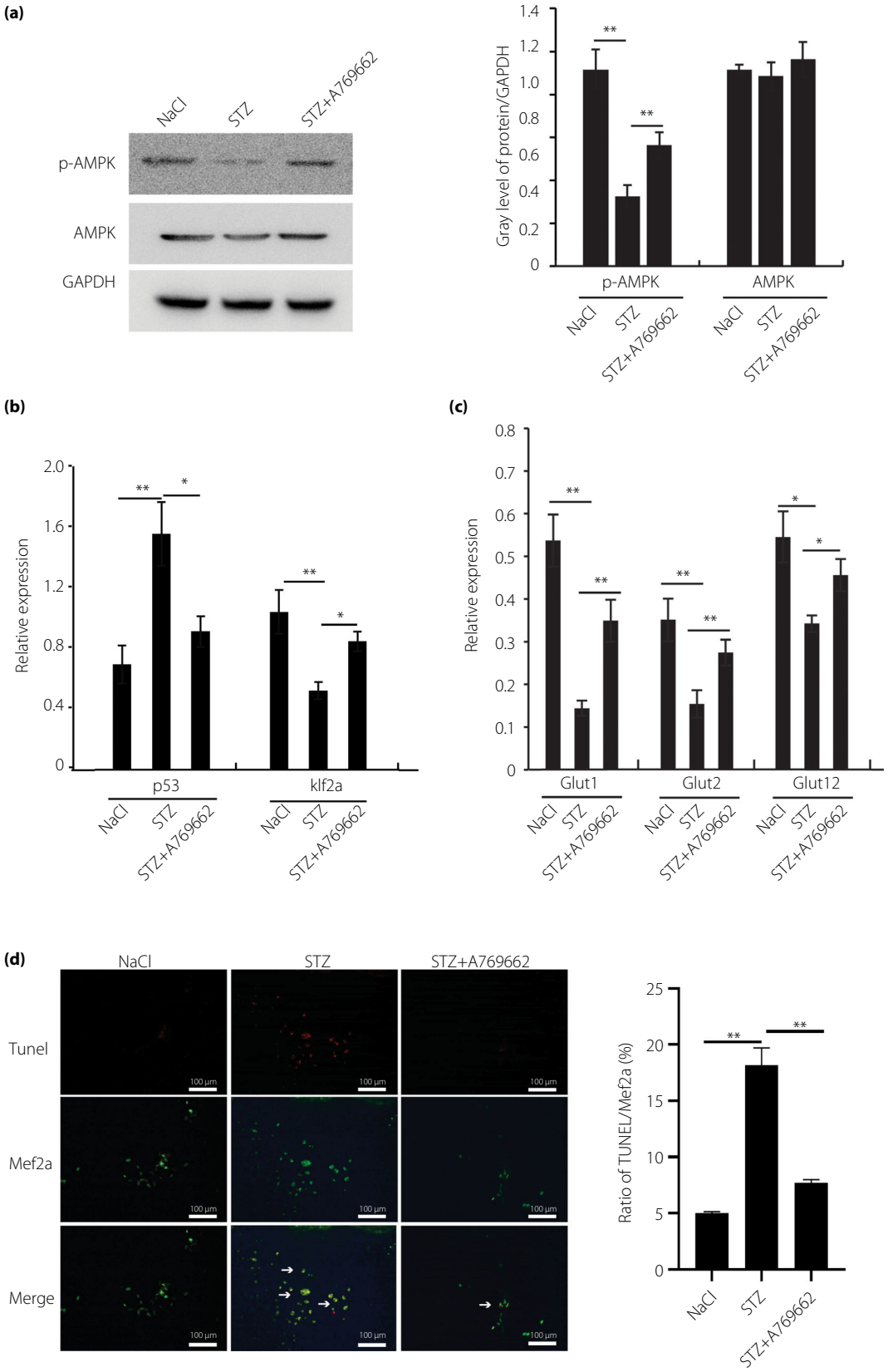
(a)
NaCl
STZ
STZ+A769662
p-AMPK
AMPK
GAPDH
Gray level of protein/GAPDH
p-AMPK
AMPK
(b)
Relative expression
p53
klf2a
(c)
Relative expression
Glut1
Glut2
Glut12
(d)
Tunel
Mef2a
Merge
100 μm
Ratio of TUNEL/Mef2a (%)

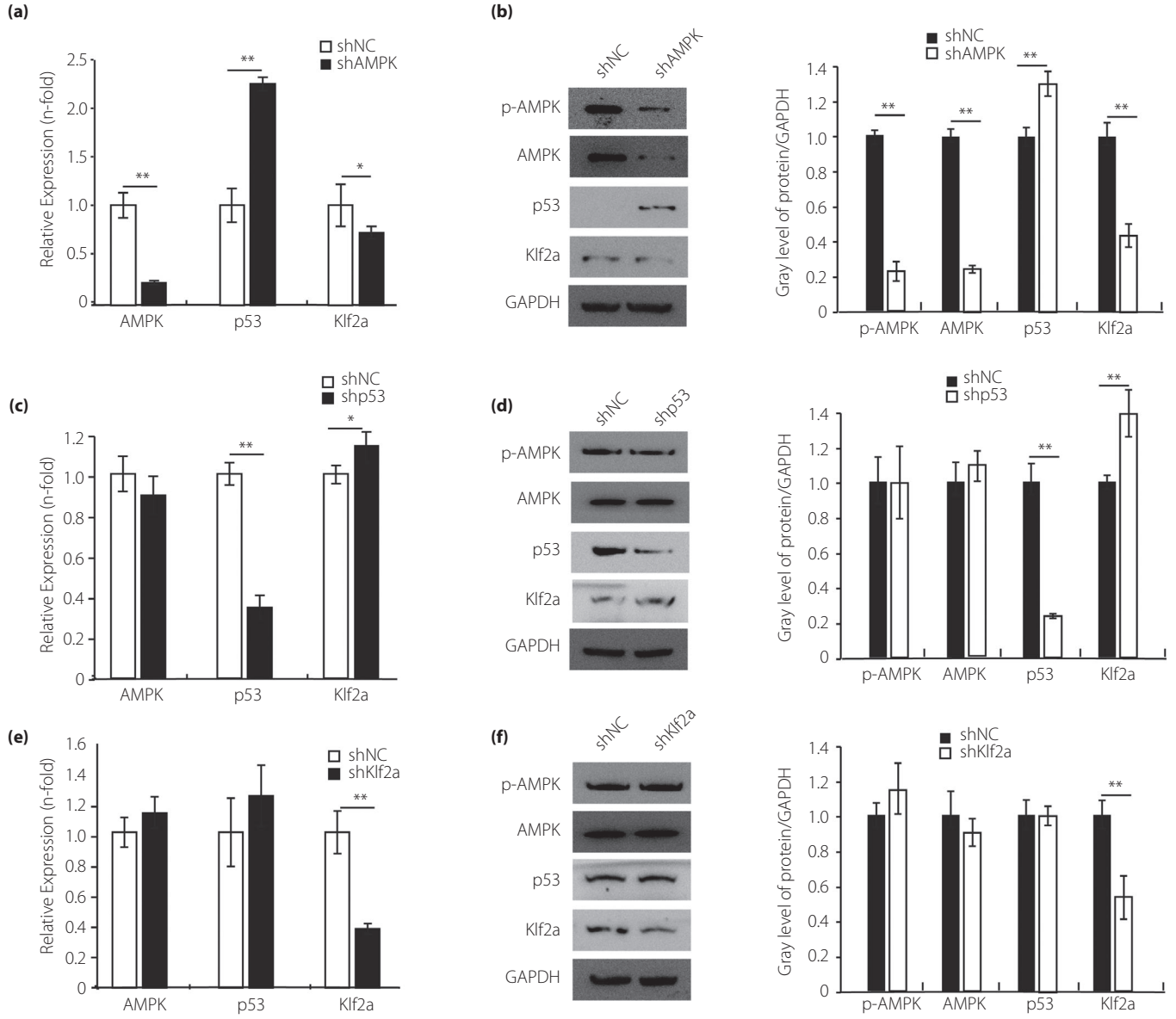

Figure 6 | The upstream and downstream relationship among the adenosine monophosphate-activated protein kinase (AMPK) pathway in the zebrafish cardiomyocytes. (a,b) Quantitative polymerase chain reaction and western blot analysis of AMPK pathway in the cardiomyocytes transfected with short hairpin AMPK (shAMPK). Glyceraldehyde 3-phosphate dehydrogenase (GAPDH) was measured as the control. (c,d) Quantitative polymerase chain reaction and western blot analysis of the AMPK pathway in the cardiomyocytes transfected with short hairpin p53 (shp53). GAPDH was measured as the control. (e,f) Quantitative polymerase chain reaction and western blot analysis of the AMPK pathway in the cardiomyocytes transfected with short hairpin klf2a (shklf2a). GAPDH was measured as the control. Each experiment was repeated a minimum of three times. *****Statistically significant difference ($P < 0.05$), ******Highly significant difference ($P < 0.01$) in a two-tailed Student's *t*-test. p-AMPK, phospho-adenosine monophosphate-activated protein kinase; STX, streptozocin.

qPCR and western blotting analysis showed that p53 expression was inhibited and klf2a expression was elevated without altering AMPK expression in the cells transfected with shp53 (Figure 6c,d). In addition, qPCR and western blotting analysis showed that klf2a expression was inhibited, but showed no alteration in the expression of AMPK and p53 in cells transfected with shklf2a (Figure 6e,f).

DISCUSSION

Our previous work included zebrafish model mimics of type 2 diabetes by inducing high glucose[33]. The blood glucose levels *in vivo* were elevated, the body mass of zebrafish treated with STZ was decreased and cardiomyopathy structural remodeling was observed in hyperglycemic zebrafish, which was consistent with the metabolic disturbances in type 1 diabetes

(Figures 1,3,4). The levels of GLUTs expression in zebrafish hearts indicated the decreased ability of zebrafish myocardium to utilize glucose. (Figure 1b,c). Studies have suggested that the changes in ECG in high-glucose models usually occurred early in the disease[38,39]. ECG results in the present study showed that the HR in high-glucose models was slowed down, which was consistent with the rodent diabetes model[40]. ECG changes occurred after 21 days of STZ injection, including ST-T changes, increased electrical alterations and QTc-interval prolongation, suggesting myocardial ischemia and impaired cardiac function. Furthermore, non-invasive ECG was used to detect cardiac function of zebrafish, and reduced results of SV, CO and EF after 21 days of STZ-intervention suggested damage of myocardial contractility in the hyperglycemic zebrafish group (Table 1). Meanwhile, after 14 days of STZ intervention, the IVRTa of the zebrafish hearts in the hyperglycemia group was shorter than the control group, whereas IVCTa showed no marked reduction, indicating diastolic dysfunction before systolic dysfunction. This was consistent with the majority of evidence on DCM[41–43], and patients with diabetes usually have impaired diastolic function followed by contraction function. Furthermore, as shown in Table 1, the variations in the early diastolic flow velocity (peak E), and the late diastolic/atrial flow velocity (peak A) and E/A ratio, are opposite to what is seen in humans and other higher vertebrates. This is probably because of the size and construction of zebrafish hearts, that are used for assessing cardiac diastolic function through E/A ratio alteration in zebrafish, are limited.

Previous studies have shown that AMPK, a sensor of cellular energy status, is involved in cell apoptosis, and its function in cell apoptosis is often controversial[36]. AMPK is considered as a key regulator of cellular and systemic energy homeostasis, and is involved in various metabolic functions in diseases. Thus, it is necessary to directly activate AMPK with the help of drugs, and understand the mechanism of its role in many diseases, such as cardiovascular disease, type 2 diabetes mellitus, obesity and cancers, as well as DCM. In the present study, AMPK expression was decreased in STZ-induced apoptosis along with apoptosis, activated p53 and suppressed klf2a (Figures 2b,3c). The present study found that A769662 could activate AMPK (Figure 2a,b), which in turn attenuates apoptosis, and restores pathological conditions and dysfunction of hyperglycemic fish model hearts (Figures 4d,3c; Table 2). Also, regulation of AMPK could affect apoptosis in CMs and the zebrafish model of hyperglycemia. Thus, ECG analysis showed activation of AMPK in hyperglycemic model zebrafish, resulting in more increased SV, CO and EF, and prolonged IVRTa and IVCTa in the AMPK-activated group than hyperglycemic zebrafish. This is an improvement in diastolic and contraction functions. Above all, activation of AMPK could inhibit remodeling of the heart. Apoptosis is defined as a programmed cell death, and exerts an important function in eliminating excessive, damaged or harmful cells. Previous studies have documented that apoptosis caused loss of contractile tissue, cardiac remodeling and dysfunction in DCM[18]. In our studies, TUNEL analysis showed that STZ induced cell apoptosis in hyperglycemic zebrafish hearts (Figure 3c), indicating that anti-apoptosis might be a potential treatment strategy for DCM. The most noteworthy point is that cardiac remodeling of the heart in hyperglycemic zebrafish was attenuated when the apoptosis was inhibited (Figure 3c). Taken together, these results suggested that the AMPK pathway might be a potentially new therapeutic target for treating DCM. It is important to understand whether upregulation of AMPK acts as a compensatory change to protect against cardiomyopathy. In summary, the results showed significant advances in the development of AMPK-targeting therapies and a reliable method to treat DCM.

Furthermore, an *in vitro* study of hyperglycemic zebrafish CMs was carried out to determine the direct effects of high glucose, and the roles of AMPK, p53 and klf2a. Messenger RNA expression of AMPK, p53 and klf2a was determined when the CMs of hyperglycemic zebrafish were incubated. To support this, the lentivirus knockdown system showed an upstream and downstream relationship among AMPK, p53 and klf2a *in vitro* CMs. qPCR and western blotting analyses showed that AMPK reversed the regulation of p53, and that p53 was considered as an upstream activator of klf2a, which is vital for the progression of hyperglycemia-induced cardiomyopathy of adult zebrafish. In summary, these results showed that apoptosis and the AMPK pathway was included in DCM, and the AMPK–P53–-klf2a pathway might be considered as a suitable method for progression, development and treatment of DCM.

We might be able to propose that intervention with AMPK activators can increase AMPK phosphorylation, which downregulates p53, then upregulates klf2a, thereby reducing apoptosis, and improving ventricular remodeling and cardiac dysfunction. The limitations of our research are as follows: the therapeutic benefit of AMPK was built on a single compound A-769662, and only one experiment was carried out on apoptosis, which should be further studied in the future.

In conclusion, a DCM model was successfully established. A new molecular pathway of the AMPK–p53–klf2a pathway plays an important role in hyperglycemia-induced cardiac remodeling in adult zebrafish, which might be regarded as a potential method to treat DCM.

ACKNOWLEDGMENTS

We thank Dr Yuehua Fang for his help with technical assistance. This research was supported by National Natural Science Foundation of China (81370331).

DISCLOSURE

The authors declare no conflict of interest.

REFERENCES

1. Gilbert RE, Krum H. Heart failure in diabetes: effects of anti-hyperglycaemic drug therapy. *Lancet* 2015; 385: 2107–2117.

2. Rubler S, Dlugash J, Yuceoglu YZ, *et al*. New type of cardiomyopathy associated with diabetic glomerulosclerosis. *Am J Cardiol* 1972; 30: 595–602.
3. Boudina S, Abel ED. Diabetic cardiomyopathy revisited. *Circulation* 2007; 115: 3213–3223.
4. Jia G, DeMarco VG, Sowers JR. Insulin resistance and hyperinsulinaemia in diabetic cardiomyopathy. *Nat Rev Endocrinol* 2016; 12: 144–153.
5. Bugger H, Abel ED. Molecular mechanisms of diabetic cardiomyopathy. *Diabetologia* 2014; 57: 660–671.
6. Gut P, Reischauer S, Stainier DY, *et al*. Little fish, big data: zebrafish as a model for cardiovascular and metabolic disease. *Physiol Rev* 2017; 97: 889–938.
7. Chávez MN, Aedo G, Fierro FA, *et al*. Zebrafish as an emerging model organism to study angiogenesis in development and regeneration. *Front Physiol* 2016; 7: 56.
8. Zeng WR, Beh SJ, Bryson-Richardson RJ, *et al*. Production of zebrafish cardiospheres and cardiac progenitor cells *in vitro* and three-dimensional culture of adult zebrafish cardiac tissue in scaffolds. *Biotechnol Bioeng* 2017; 114: 2142–2148.
9. Benam KH, Dauth S, Hassell B, *et al*. Engineered *in vitro* disease models. *Annu Rev Pathol* 2015; 10: 195–262.
10. Zuo G, Ren X, Qian X, *et al*. Inhibition of JNK and p38 MAPK-mediated inflammation and apoptosis by ivabradine improves cardiac function in streptozotocin-induced diabetic cardiomyopathy. *J Cell Physiol* 2019; 234: 1925–1936.
11. Pei Z, Deng Q, Babcock SA, *et al*. Inhibition of advanced glycation endproduct (AGE) rescues against streptozotocin-induced diabetic cardiomyopathy: role of autophagy and ER stress. *Toxicol Lett* 2018; 284: 10–20.
12. Kanter M, Aksu F, Takir M, *et al*. Effects of low intensity exercise against apoptosis and oxidative stress in Streptozotocin-induced diabetic rat heart. *Exp Clin Endocrinol Diabetes* 2017; 125: 583–591.
13. Sarras MP Jr, Leontovich AA, Olsen AS, *et al*. Impaired tissue regeneration corresponds with altered expression of developmental genes that persists in the metabolic memory state of diabetic zebrafish. *Wound Repair Regen* 2013; 21: 320–328.
14. Pan Y, Wang Y, Zhao Y, *et al*. Inhibition of JNK phosphorylation by a novel curcumin analog prevents high glucose-induced inflammation and apoptosis in cardiomyocytes and the development of diabetic cardiomyopathy. *Diabetes* 2014; 63: 3497–3511.
15. Liu Z, Zhao N, Zhu H, *et al*. Circulating interleukin-1β promotes endoplasmic reticulum stress-induced myocytes apoptosis in diabetic cardiomyopathy via interleukin-1 receptor-associated kinase-2. *Cardiovasc Diabetolo* 2015; 14: 125.
16. Wang Y, Feng W, Xue W, *et al*. Inactivation of GSK-3beta by metallothionein prevents diabetes-related changes in cardiac energy metabolism, inflammation, nitrosative damage, and remodeling. *Diabetes* 2009; 58: 1391–1402.
17. Cai L, Wang Y, Zhou G, *et al*. Attenuation by metallothionein of early cardiac cell death via suppression of mitochondrial oxidative stress results in a prevention of diabetic cardiomyopathy. *J Am Coll Cardiol* 2006; 48: 1688–1697.
18. Ren XM, Zuo GF, Wu W, *et al*. Atorvastatin alleviates experimental diabetic cardiomyopathy by regulating the GSK-3beta-PP2Ac-NF-kappaB signaling axis. *PLoS One* 2016; 11: e0166740.
19. Li S, Zhang L, Ni R, *et al*. Disruption of calpain reduces lipotoxicity-induced cardiac injury by preventing endoplasmic reticulum stress. *Biochim Biophys Acta* 2016; 1862: 2023–2033.
20. Yu H, Zhen J, Yang Y, *et al*. Ginsenoside Rg1 ameliorates diabetic cardiomyopathy by inhibiting endoplasmic reticulum stress-induced apoptosis in a streptozotocin-induced diabetes rat model. *J Cell Mol Med* 2016; 20: 623–631.
21. Hardie DG, Carling D, Carlson M. The AMP-activated/SNF1 protein kinase subfamily: metabolic sensors of the eukaryotic cell? *Annu Rev Biochem* 1998; 67: 821–855.
22. Shackelford DB, Shaw RJ. The LKB1-AMPK pathway: metabolism and growth control in tumour suppression. *Nat Rev Cancer* 2009; 9: 563–575.
23. Guo S, Yao Q, Ke Z, *et al*. Resveratrol attenuates high glucose-induced oxidative stress and cardiomyocyte apoptosis through AMPK. *Mol Cell Endocrinol* 2015; 412: 85–94.
24. Monteverde T, Muthalagu N, Port J, *et al*. Evidence of cancer-promoting roles for AMPK and related kinases. *FEBS J* 2015; 282: 4658–4671.
25. Dekker RJ, van Soest S, Fontijn RD, *et al*. Prolonged fluid shear stress induces a distinct set of endothelial cell genes, most specifically lung Kruppel-like factor (KLF2). *Blood* 2002; 100: 1689–1698.
26. Parmar KM, Larman HB, Dai G, *et al*. Integration of flow-dependent endothelial phenotypes by Kruppel-like factor 2. *J Clin Investig* 2006; 116: 49–58.
27. Wang F, Zhu Y, Huang Y, *et al*. Transcriptional repression of WEE1 by Kruppel-like factor 2 is involved in DNA damage-induced apoptosis. *Oncogene* 2005; 24: 3875–3885.
28. Chu CY, Chen CF, Rajendran RS, *et al*. Overexpression of Akt1 enhances adipogenesis and leads to lipoma formation in zebrafish. *PLoS One* 2012; 7: e36474.
29. Sun Y, Fang Y, Xu X, *et al*. Evidence of an association between age-related functional modifications and pathophysiological changes in zebrafish heart. *Gerontology* 2015; 61: 435–447.
30. Huang WC, Hsieh YS, Chen IH, *et al*. Combined use of MS-222 (tricaine) and isoflurane extends anesthesia time and minimizes cardiac rhythm side effects in adult zebrafish. *Zebrafish* 2010; 7: 297–304.

31. Sander V, Sune G, Jopling C, *et al*. Isolation and *in vitro* culture of primary cardiomyocytes from adult zebrafish hearts. *Nat Protoc* 2013; 8: 800–809.
32. Janjuha S, Pal Singh S, Ninov N. Analysis of beta-cell function using single-cell resolution calcium imaging in zebrafish islets. *J Vis Exp* 2018: https://doi.org/10.3791/57851
33. Sun Y, Wang Q, Fang Y, *et al*. Activation of the Nkx2.5-Calr-p53 signaling pathway by hyperglycemia induces cardiac remodeling and dysfunction in adult zebrafish. *Dis Model Mech* 2017; 10: 1217–1227.
34. Zawacka-Pankau J, Grinkevich VV, Hunten S, *et al*. Inhibition of glycolytic enzymes mediated by pharmacologically activated p53: targeting Warburg effect to fight cancer. *J Biol Chem* 2011; 286: 41600–41615.
35. Duval F, Santos ED, Poidatz D, *et al*. Adiponectin inhibits nutrient transporters and promotes apoptosis in human villous cytotrophoblasts: involvement in the control of fetal growth. *Biol Reprod* 2016; 94: 111.
36. Zhang Q, Zheng S, Wang S, *et al*. Chlorpyrifos induced oxidative stress to promote apoptosis and autophagy through the regulation of miR-19a-AMPK axis in common carp. *Fish Shellfish Immunol* 2019; 93: 1093–1099.
37. Law BY, Chan WK, Xu SW, *et al*. Natural small-molecule enhancers of autophagy induce autophagic cell death in apoptosis-defective cells. *Sci Rep* 2014; 4: 5510.
38. Tougouma SJ, Kambire Y, Bado J, *et al*. Electrocardiography coupled with transthoracic echocardiography at rest in the diagnosis of cardiac impairments in type 2 diabetics: lessons learned from a cross-sectional case series in Burkina Faso. *Pan Afr Med J* 2018; 31: 169.
39. Vukomanovic V, Tadic M, Suzic-Lazic J, *et al*. The relationship between heart rate variability and left ventricular layer-specific deformation in uncomplicated diabetic patients. *Int J Cardiovasc Imaging* 2017; 33: 481–490.
40. Li X, Jiang YH, Jiang P, *et al*. Effect of Guizhi Decoction ([symbols; see text]) on heart rate variability and regulation of cardiac autonomic nervous imbalance in diabetes mellitus rats. *Chin J Integr Med* 2014; 20: 524–533.
41. Shang Y, Zhang X, Leng W, *et al*. Increased fractal dimension of left ventricular trabeculations is associated with subclinical diastolic dysfunction in patients with type-2 diabetes mellitus. *Int J Cardiovasc Imaging* 2019; 35: 665–673.
42. Graneli C, Hicks R, Brolen G, *et al*. Diabetic cardiomyopathy modelling using induced pluripotent stem cell derived cardiomyocytes: recent advances and emerging models. *Stem Cell Rev* 2019; 15: 13–22.
43. Werner RA, Eissler C, Hayakawa N, *et al*. Left ventricular diastolic dysfunction in a rat model of diabetic cardiomyopathy using ECG-gated (18)F-FDG PET. *Sci Rep* 2018; 8: 17631.